

Neutron scattering study of the vibrations in vitreous silica and germania

E. Fabiani

Institute Laue-Langevin, BP 156, F-38042 Grenoble Cedex 9, France

A. Fontana

*Dipartimento di Fisica, Università di Trento, I-38050, Povo (Trento),
Italy and INFN CRS-SOFT, c/o Università di Roma La Sapienza, I-00185, Roma, Italy*

U. Buchenau*

*Institut für Festkörperforschung, Forschungszentrum Jülich
Postfach 1913, D-52425 Jülich, Federal Republic of Germany*

(Dated: February 8, 2005)

The incoherent approximation for the determination of the vibrational density of states of glasses from inelastic neutron or x-ray scattering data is extended to treat the coherent scattering. The method is applied to new room temperature measurements of vitreous silica and germania on the thermal time-of-flight spectrometer IN4 at the High Flux Reactor in Grenoble. The inelastic dynamic structure factor at the boson peak turns out to be reasonably well described in terms of a mixture of rotation and translation of practically undistorted SiO_4 or GeO_4 tetrahedra. The translational component exceeds the expectation of the Debye model by a factor of two. A possible relation of this excess to the phonon shift and broadening observed in x-ray Brillouin scattering experiments is discussed.

PACS numbers: 63.50.+x, 64.70.Pf

I. INTRODUCTION

There is an extensive quantum mechanical treatment of the scattering from atoms moving in a crystal¹. The regular atomic arrangement allows to solve this problem with an accuracy and a theoretical depth which one cannot hope for in the much more complex case of a disordered solid. In a glass, the translation symmetry is lost. In addition, the sample is in an energy landscape with many minima. Fortunately, the relaxational jumps between different energy minima of glasses are only seen as quasielastic scattering below an energy transfer of about $1 \text{ meV}^{2,3}$ (a frequency of 250 GHz); above that frequency, one can reckon with a more or less harmonic vibrational density of states.

But the problem what these vibrations are is by no means solved. Below 1 meV, reasonably well-defined long-wavelength sound waves can be shown to exist (co-existing with relaxational or tunneling motion), but they become rapidly overdamped above that frequency. This was first deduced⁴ from the plateau in the thermal conductivity at low temperatures. Within the last decade, it has been directly observed for the longitudinal sound waves by x-ray Brillouin scattering⁵. Also, the density of states exceeds the Debye expectation markedly at the so-called boson peak, at a frequency where the corresponding crystals still have only well-defined long-wavelength sound waves.

In this paper, we report thermal neutron time-of-flight measurements at room temperature on silica and germania, data taken over a very large momentum transfer range with the new spectrometer IN4 at the High Flux Reactor at the Institut Laue-Langevin at Grenoble. The

high quality of the data allows for an evaluation which goes beyond the usual incoherent approximation, extending and improving earlier work^{6,7,8,9,10}. One not only gets a vibrational density of states which compares favorably with heat capacity data, but one learns new facts on the details of the atomic motion, in particular in the low-frequency range at the boson peak.

After this introduction, the paper describes an extension of the incoherent approximation for the evaluation of coherent inelastic neutron or x-ray data in Section II. Section III presents the time-of-flight experiments in silica and germania, their multiple-scattering correction and their normalization to diffraction data from the literature. Section IV applies the new method to the data. The discussion of the results and a short summary is given in Sections V and VI.

II. EXTENDING THE INCOHERENT APPROXIMATION

A. Definitions

The following derivation is formulated in terms of the classical scattering law $S(Q, \omega)$, where the frequency ω is related to the energy transfer E of the scattering process by $E = \hbar\omega$ and Q is the momentum transfer. This classical $S(Q, \omega)$ can be calculated from the measured double differential cross section

$$S(Q, \omega) = \frac{k_B T}{\hbar\omega} (e^{\hbar\omega/k_B T} - 1) \frac{k_i}{k_f} \frac{4\pi}{N\bar{\sigma}} \frac{d^2\sigma}{d\omega d\Omega}, \quad (1)$$

taking ω to be positive in energy gain of the scattered particle, neutron or x-ray photon. Here T is the temperature, k_i and k_f are the wavevector values of incoming and scattered waves, respectively, N is the number of atoms in the beam, $\bar{\sigma}$ is the average scattering cross section of the atoms and Ω is the solid angle. Note that the average scattering cross section $\bar{\sigma}$ is Q -dependent for x-rays; this Q -dependence is determined by the atomic form factors. The definition of $S(Q, \omega)$ requires a completely isotropic glass, the usual case. It is also valid for glasses with more than one kind of atom, like silica and germania.

The above definition makes no distinction between coherent scattering (the case where the waves scattered from different atoms interfere) and incoherent scattering (the case where there is no interference). X-ray scattering is purely coherent; for neutrons, it depends on the nuclei of the scattering atoms. In silicon, germanium and oxygen atoms, the coherent scattering dominates. Integrating over all frequencies one obtains $S(Q)$

$$S(Q) \equiv \int_{-\infty}^{\infty} d\omega S(Q, \omega). \quad (2)$$

If all atoms of the sample scatter only incoherently, $S(Q) = 1$. If one has only coherent scattering, $S(Q)$ shows a first sharp diffraction peak at about 1.5 Å, followed by oscillations around 1 which die out at high Q . These peaks reflect the short range order of the glass on the atomic scale. Below the first sharp diffraction peak, $S(Q)$ is due to long-range density and concentration fluctuations. Silica and germania show a pronounced first sharp diffraction peak.

For the evaluation of coherent scatterers, we will need the definition of a hypothetical incoherent scattering function $S_{inc}(Q, \omega)$. This is defined as the scattering function which one would have without interference between different atoms, keeping their total cross sections.

B. The incoherent approximation

To determine a vibrational density of states from scattering data, one needs to take the Debye-Waller factor and the multiphonon scattering into account. An elegant way to do this is to use the intermediate scattering function

$$S(Q, t) = \int_{-\infty}^{\infty} \cos \omega t S(Q, \omega) d\omega. \quad (3)$$

with the back transform

$$S(Q, \omega) = \frac{1}{\pi} \int_0^{\infty} \cos \omega t S(Q, t) dt, \quad (4)$$

The incoherent approximation assumes that one can describe the scattering function, eq. (1), in terms of an average atom which scatters only incoherently. The time-dependent displacement of this average atom from

its equilibrium position is assumed to have a Gaussian distribution. From the Bloch identity¹, one obtains the intermediate scattering function

$$S_{inc}(Q, t) = e^{-Q^2 \gamma(t)}, \quad (5)$$

where $\gamma(t)$ is the time-dependent mean square displacement of the average atom.

If there are only vibrations, $\gamma(t)$ is determined by the vibrational density of states $g(\omega)$. Their relation can be derived from the one-phonon approximation for the inelastic scattering from our classical isotropic incoherent scatterer¹

$$S_{inc}(Q, \omega) = Q^2 e^{-2W} \frac{k_B T}{2\bar{M}} \frac{g(\omega)}{\omega^2} \quad (6)$$

where e^{-2W} is the Debye-Waller factor and \bar{M} is the average atomic mass. Comparing the initial Q^2 rise and using the Fourier transformation, eq. (3), one finds

$$\gamma(t) = \frac{k_B T}{\bar{M}} \int_0^{\omega_{max}} d\omega \frac{g(\omega)}{\omega^2} (1 - \cos \omega t). \quad (7)$$

Here ω_{max} is the upper frequency boundary of the vibrational density of states.

The incoherent scattering is obtained from the Fourier transform of the intermediate scattering function in time

$$S_{inc}(Q, \omega) = \frac{1}{\pi} \int_0^{\infty} dt \cos \omega t e^{-\gamma(t) Q^2}. \quad (8)$$

In this approximation, one accounts not only for the one-phonon scattering, but the entire inelastic scattering including the multiphonon terms.

To apply the approximation to measured data, one begins by calculating a first guess to the vibrational density of states, assuming a Q^2 - or $Q^2 e^{-2W}$ -dependence of the inelastic scattering. From the density of states, one gets $\gamma(t)$ from eq. (7) and can calculate the Q -dependence of the inelastic scattering. With this, one can determine a better density of states from the data. Usually, after a few iterations the density of states does no longer change. In the case of a glass consisting of two or more elements, one calls this density the *generalized vibrational density of states*, to emphasize that it is not the true density of states, but its reflection in the scattering, weighted by the cross sections and masses of the atoms in the sample.

As we will see, the incoherent approximation works astonishingly well even for the two coherently scattering glasses silica and germania. But it does not provide any information on the vibrational eigenvectors. One needs an extension of the incoherent approximation to do that. Such an extension will be introduced in the following subsection.

C. Oscillation function $S_{\omega}(Q)$

The vibrational density of states is a function of the frequency, not of the time. Therefore the extension of

the incoherent approximation must be done in the frequency domain. The vibrational eigenvectors change with changing frequency, so each frequency window has its own coherent dynamic structure factor. The interference between different scattering atoms does not change the overall scattering intensity, but leads to oscillations in the dependence on the momentum transfer.

To take this into account, we define the oscillation function $S_\omega(Q)$ by

$$S_\omega(Q) = \frac{S(Q, \omega)}{S_{inc}(Q, \omega)}, \quad (9)$$

where $S_{inc}(Q, \omega)$ is understood to be the scattering function without interference between different atoms, but with unchanged total cross sections, as defined in II. A.

Like $S(Q)$, $S_\omega(Q)$ equals 1 in the incoherent case. It is an extension of $S(Q)$ to describe the coherent oscillations of the scattering at a fixed frequency ω , both for elastic and inelastic scattering. Though our main interest is in the inelastic part, it is suitable to begin the discussion with the elastic part $S_0(Q)$ for $\omega = 0$.

As $S(Q)$ reflects the pair correlation of the atoms in their instantaneous positions, the elastic oscillation function $S_0(Q)$ reflects the pair correlation of the atoms in their equilibrium positions. In a glass at low temperatures (and even at not so low temperatures), the atomic displacements are small compared to the interatomic distances, so $S_0(Q) \approx S(Q)$. Both functions show the first sharp diffraction peak at about 1.5 Å followed by further peaks at higher momentum transfer. At still higher momentum transfer, the peak amplitudes diminish and the functions $S(Q)$ and $S_0(Q)$ approach the final value of 1. Below the first sharp diffraction peak, at small momentum transfer, $S_0(Q)$ mirrors the frozen density and concentration fluctuations of the glass, while $S(Q)$ mirrors both static and dynamic ones.

The inelastic part of the oscillation function $S_\omega(Q)$ with $\omega \neq 0$ will depend on the vibrational modes at the given frequency. At small momentum transfer, it shows the Brillouin peak, the scattering from longitudinal sound waves. The interference pattern at higher momentum transfer is not only due to the positional phase factors which determine $S(Q)$, but also to the scalar product of momentum transfer and atomic displacement (see eq. (11)). Thus the inelastic part of $S_\omega(Q)$ contains information on the eigenvectors of the vibrational modes at the frequency ω .

With the help of the oscillation function, the incoherent approximation, eq. (8), transforms into the extended approximation

$$S(Q, \omega) = S_\omega(Q) \frac{1}{\pi} \int_0^\infty dt \cos \omega t e^{-\gamma(t)Q^2}. \quad (10)$$

The approximation allows to fit not only a density of states, but a frequency-dependent oscillation function as well. Thus, for coherent scatterers, the introduction of $S_\omega(Q)$ provides not only an enormous reduction of the

deviation between incoherent approximation and experiment, but opens up the possibility to analyze the vibrational eigenvectors^{6,8}. If this analysis is successful, one can proceed to calculate the true vibrational density of states, because then one knows the weight of a given mode in the scattering.

In the harmonic one-phonon approximation, one can express the coherent inelastic scattering¹ from a given normal mode in terms of its eigenvector \mathbf{e}_j , the equilibrium position \mathbf{r}_j and the scattering length b_j of atom j , ($j = 1..N$) (the scattering length b_j is related to the coherent cross section σ_j by $\sigma_j = 4\pi b_j^2$). Within the one-phonon approximation, the oscillation function

$$S_\omega(Q) = \left\langle \frac{3}{Q^2 F_{norm}} \left| \sum_{j=1}^N b_j e^{-i\mathbf{Q}\mathbf{r}_j} \frac{\mathbf{Q}\mathbf{e}_j}{M_j^{1/2}} \right|^2 \right\rangle_\omega, \quad (11)$$

where the angular brackets denote an average over all eigenmodes at the frequency ω , together with a directional average over the momentum transfer vector \mathbf{Q} . The mode normalization factor F_{norm} is given by

$$F_{norm} = \sum_{j=1}^N \frac{b_j^2 \mathbf{e}_j^2}{M_j}. \quad (12)$$

If one is able to find the proper mode eigenvectors, one can go beyond the determination of a generalized vibrational density of states, because the proper normalization factor contains cross sections and masses and thus allows to determine the true vibrational density of states. This paper aims at such a treatment for the silica and germania measurements described in the next section.

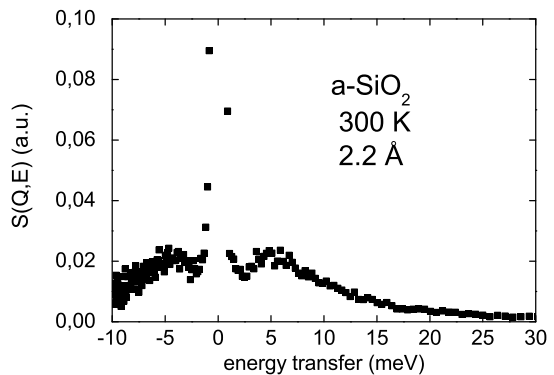


FIG. 1: IN4 spectrum (with standard corrections) from vitreous silica at a scattering angle of 104 degrees, showing the boson peak at both sides of the elastic line.

III. EXPERIMENT

A. Samples and time-of-flight experiment

The vitreous silica sample used for the IN4 experiments was a commercial grade spectro-sil disk with a diameter of 50 mm and a thickness of 4.8 mm.

In the case of vitreous germania, appropriate amounts of reagent-grade GeO_2 powder (Aldrich 99.99+%) were melted in platinum crucibles for about 1 h at ca. 1600 C. The homogeneous and bubble-free melt was subsequently quenched in water and glassy samples of irregular shape were removed from the bottom of the crucible. This preparation technique results in completely transparent glasses. Several such pieces were arranged to mimic the disk shape of the silica sample.

The neutron spectra were obtained on the thermal time-of-flight spectrometer IN4 at the High Flux Reactor of the Institut Laue-Langevin at Grenoble. The measurements were done in reflection geometry, with the sample disk plane inclined at 45 degrees to the incoming beam. With a wavelength of incoming neutrons of 1.53 Å, one is able to study the momentum transfer range from 1.5 to 7 Å⁻¹ with an energy resolution of 1.3 meV FWHM. Similarly, a wavelength of incoming neutrons of 2.2 Å allowed to study the momentum transfer range from 1 to 4.9 Å⁻¹ with an energy resolution of 0.8 meV FWHM.

The momentum transfer range of these measurements is more than a factor of two larger than the one of earlier investigations^{6,8} with cold neutrons on the time-of-flight spectrometer IN6. One of these earlier measurements (vitreous silica at 318 K) was included in the evaluation presented below.

The IN4 measurements were performed at temperatures between 5 and 300 K. The following evaluation, however, is restricted to the 300 K data.

B. Corrections

The measured neutron counts were corrected for the empty container signal. The detector efficiency was corrected for by a measurement of a vanadium sample (an incoherent scatterer) in the same container. The signal was multiplied by k_i/k_f and an angle-dependent absorption correction was calculated. These four standard corrections were done with the program INX of the Institut Laue-Langevin at Grenoble. Fig. 1 shows such a corrected spectrum for silica at the highest scattering angle.

The multiple scattering correction was done assuming an angle-independent multiple scattering contribution. For silica and germania, where wide-angle scattering predominates, this assumption is expected to hold.

To do the correction, one first calculates an average spectrum, weighting each detector with the sine of its scattering angle. This spectrum should be folded with it-

self to get the spectrum of the twice-scattering processes. However, to treat the elastic line correctly, one has to replace the elastic line by a δ -function in one of the two spectra which one folds. Otherwise the procedure would broaden the elastic line in an unphysical way.

The question how much of the resulting twice-scattering spectrum one should subtract is answered by looking at the momentum transfer dependence in the inelastic part of the spectrum. On a normalized scale, one subtracts a fraction s_{mu} , chosen in such a way that the inelastic intensity extrapolates to zero towards zero momentum transfer. As an example, Fig. 2 shows corrected (with $s_{mu} = 0.1$) and uncorrected data for germania at 300 K between 1 and 5 meV, measured with incoming neutrons of a wavelength of 2.2 Å.

The procedure is not exact, because the coherent inelastic scattering at small momentum transfer is not exactly zero. If the velocity of the incoming neutrons exceeds the longitudinal sound velocity of the glass (the kinematic condition¹ for the visibility of the Brillouin line), one sees the Brillouin scattering. But even if it does not (as in the measurements reported here), there is still a small nonzero coherent inelastic scattering contribution. This, however, is small compared to the multiple scattering^{11,12}.

C. Normalization to $S(Q)$

In principle, if one does all corrections properly, one should be able to normalize the measurement to the vanadium signal. In practice, it is easier and more accurate to normalize the time-of-flight data of a glass to the $S(Q)$ of a diffraction measurement. For vitreous silica, there are two such diffraction measurements in the literature^{13,14}. They agree very well with each other. For germania, there is only one diffraction measurement¹⁵.

To determine $S(Q)$ from a time-of-flight dataset, one

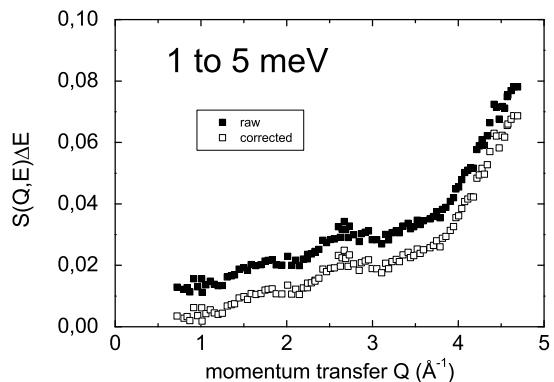


FIG. 2: Inelastic signal from 1 to 5 meV for germania at 300 K, incoming wavelength 2.2 Å, with and without multiple scattering correction.

integrates the scattering over the time channels of a single detector or a detector group, correcting for the change in momentum transfer as the energy transfer changes. Here, we corrected with the factor Q_{el}^2/Q^2 , where Q_{el} is the momentum transfer at the elastic line and Q is the one at finite energy transfer. The procedure is not exact, but it has the advantage that a bad detector does not corrupt its neighbors.

Fig. 3 (a) shows the result of this normalization to $S(Q)$ for the two IN4 measurements on vitreous silica at room temperature. Also included is an earlier IN6 measurement⁸, done with incoming neutrons of a wavelength 4.1 Å at 318 K.

The same normalization of the two IN4 room temperature measurements of vitreous germania to diffraction data from this substance¹⁵ is shown in Fig. 3 (b). The 1.5 Å measurement suffers from problems with the subtraction of the empty container; it consisted of pure aluminum with large crystalline grains.

The comparison to Fig. 3 (a) shows that the second and the third peak in $S(Q)$ shift to lower momentum transfer in germania. This is caused by the increased Ge-O distance (1.73 Å) in germania¹⁵ as compared to the Si-O distance of 1.6 Å in silica¹³. The corner-connected GeO_4 -tetrahedra in germania are larger than the SiO_4

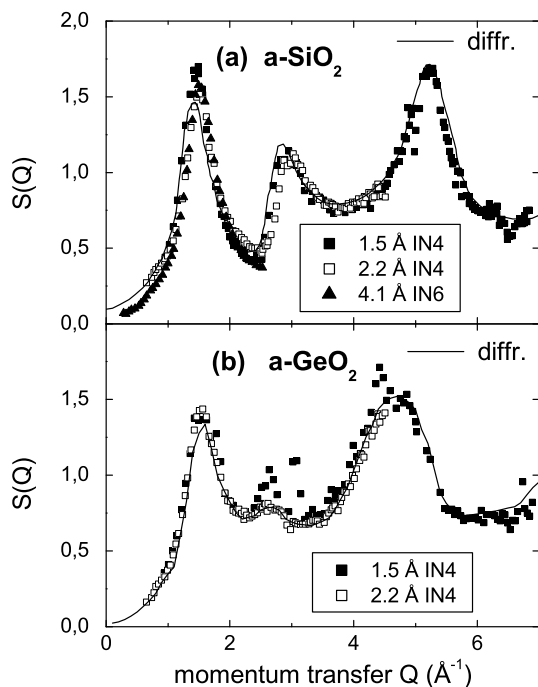


FIG. 3: (a) Normalization of IN4 data at 2.2 Å and 1.5 Å to the $S(Q)$ of vitreous silica^{13,14} (continuous line). An earlier IN6 measurement⁸ at 4.1 Å is also included (b) Normalization of IN4 data at 2.2 Å and 1.5 Å to the $S(Q)$ of vitreous germania¹⁵ (continuous line).

ones in silica. Nevertheless, the position of the first sharp diffraction peak is more or less the same in both substances, which shows that the packing of the tetrahedra must be different.

The normalization allows to compare different measurements in the same frequency window. Fig. 4 (a) shows the boson peak frequency window from 2 to 6 meV in vitreous silica for all three sets of data. One sees pronounced oscillations around the dashed line (calculated from the incoherent approximation as explained in Section III.A). Germania shows rather similar oscillations in the same window in Fig. 4 (b) (its boson peak is also at ≈ 4 meV). The task of the next section is to extract the information content in these oscillations.

As one goes up in energy transfer, the amplitude of the oscillations decreases gradually. This development is shown for vitreous silica in Fig. 5 (a-c). Above 40 meV, one finds the incoherent approximation to be valid within the experimental error. In vitreous germania, the incoherent approximation is reached even faster, around 30 meV. In both cases, there is no discernible peak shift; within experimental error, the peaks merely fade away with increasing energy transfer.

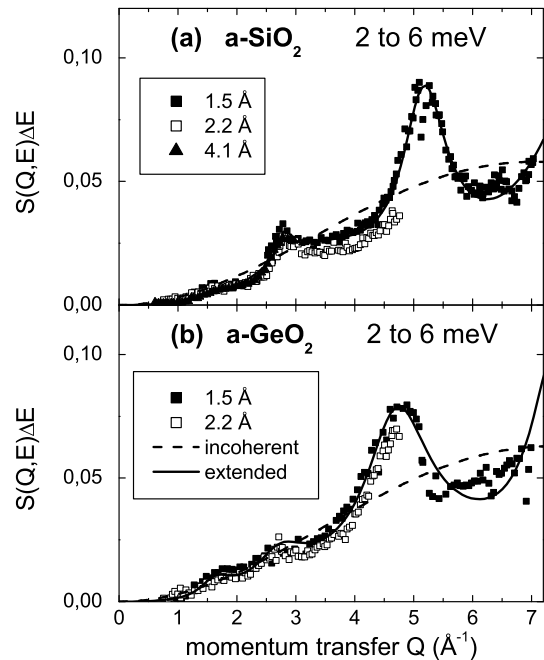


FIG. 4: The inelastic dynamic structure factor in the boson peak region from (a) the three measurements of vitreous silica (b) the two measurements of vitreous germania. The dashed line is the incoherent approximation discussed in Section III.A, the continuous line the extension to coherent scattering in terms of the empirical five-lorentzian fit explained in Section III.B.

IV. EVALUATION

A. Incoherent approximation

Having data corrected for multiple scattering and normalized to $S(Q)$, one can proceed to apply the incoherent approximation described in Section II.B. In this way, one determines a generalized vibrational density of states $g(E)$ (we replace the frequency ω by the energy transfer $E = \hbar\omega$ in this section) without any adaptable parameter.

In both cases, silica and germania, the procedure described in section II.B converged to a final generalized vibrational density of states after three iteration steps.

As it turns out, the three results for $g(E)$ of vitreous silica agree fairly well with each other. The boson peak in $g(E)/E^2$ is slightly lower in the 2.2 Å measurement, but this is not due to the oscillations of the inelastic dynamic structure factor. Looking at Fig. 4 (a), one sees that the normalized intensity itself is slightly lower than in the

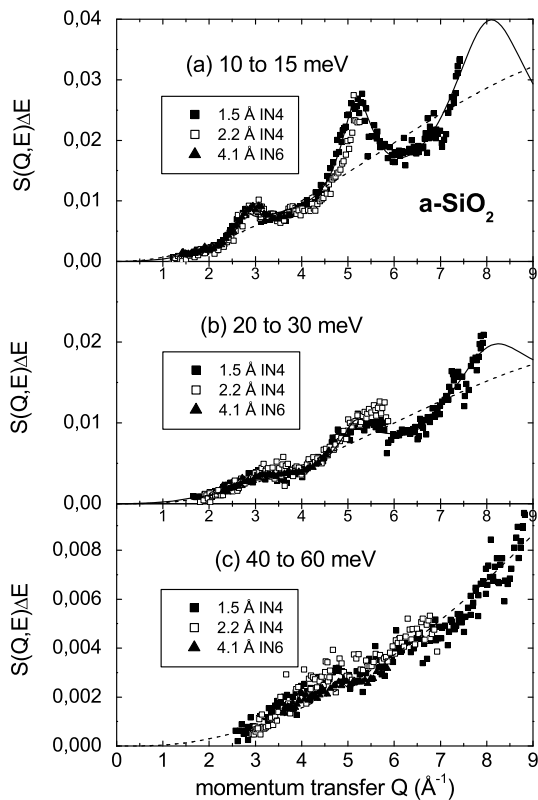


FIG. 5: The development of the inelastic dynamic structure factor of vitreous silica above the boson peak. The dashed line is the incoherent approximation discussed in Section III.A, the continuous line the extension to coherent scattering in terms of eq. (15). (a) Energy transfer from 10 to 15 meV (b) Energy transfer from 20 to 30 meV (c) Energy transfer from 40 to 60 meV.

two other measurements.

The same good agreement was found for the vibrational densities of states of germania calculated for the IN4 measurements at 1.5 and 2.2 Å.

B. Analysis of the inelastic dynamic structure factor

As the following analysis shows, we have at present no perfect eigenmode fit of the dynamic structure factor at the boson peak. Therefore we do the analysis in two steps. We first fit the oscillation function $S_{boson}(Q)$ at the boson peak in a purely empirical way with five lorentzians, independent of any motional model, but providing an excellent fit. This fit form is used to investigate the frequency dependence of the peaks in $S_{\omega}(Q)$ to higher frequencies. The second step models the atomic motion at the boson peak in terms of a sum of translation and rotation of undistorted tetrahedra. In this procedure, one has only one fit parameter (the translational fraction of the motion). One gets a reasonable rather than a perfect fit, but one has a motional model which allows to calculate the true rather than the generalized vibrational density of states.

To go beyond the incoherent approximation, we start

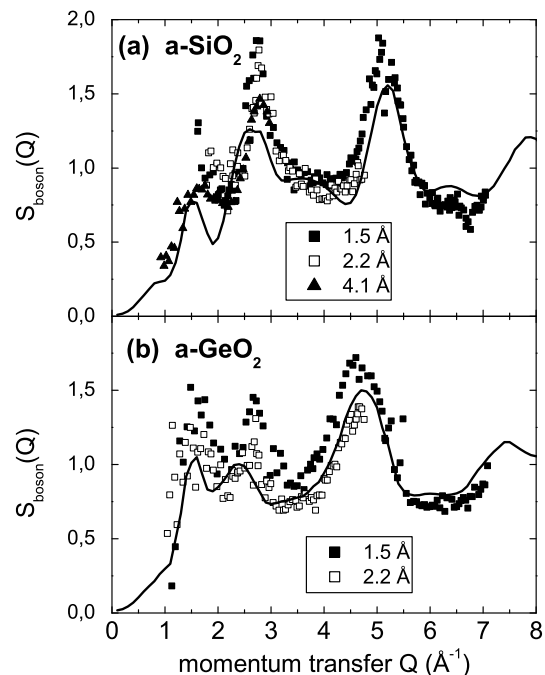


FIG. 6: Inelastic dynamic structure factor $S_{boson}(Q)$ in the boson peak region for (a) silica (continuous line sum of 0.45 $S(Q)$ and 0.55 tetrahedra libration, see text) (b) germania (continuous line sum of 0.75 $S(Q)$ and 0.25 tetrahedra libration).

by calculating the oscillation function $S_\omega(Q)$ at the boson peak via

$$S_{boson}(Q) = \frac{S_{boson}(Q, \omega)}{1/\pi \int_0^\infty dt \cos \omega t e^{-\gamma(t)Q^2}}, \quad (13)$$

taking $\gamma(t)$ from the evaluation in terms of the incoherent approximation described in the previous subsection. $S_{boson}(Q, \omega)$ is determined from the measured $S(Q, \omega)$ via

$$S_{boson}(Q, \omega) = \frac{\int_{\omega_{min}}^{\omega_{max}} S(Q, \omega) d\omega}{\omega_{max} - \omega_{min}}, \quad (14)$$

where $\hbar\omega_{min}=2$ meV was chosen to exclude any contribution of the elastic line even for the 1.53 Å measurement and $\hbar\omega_{max}=6$ meV is a frequency well above the two boson peak frequencies of 4 meV and 3.6 meV for silica and germania, respectively. Fig. 6 (a) shows the result for the three sets of data of silica, Fig. 6 (b) for the two IN4 measurements of germania.

The next step is to quantify the fading-away of the oscillations with increasing frequency. For this, we need a functional expression for $S_{boson}(Q)$. To get it, we fit the data points of Fig. 6 (a) in terms of a sum of five lorentzians (the continuous line in Fig. 6 (a)). This purely empirical function oscillates around 1 in the

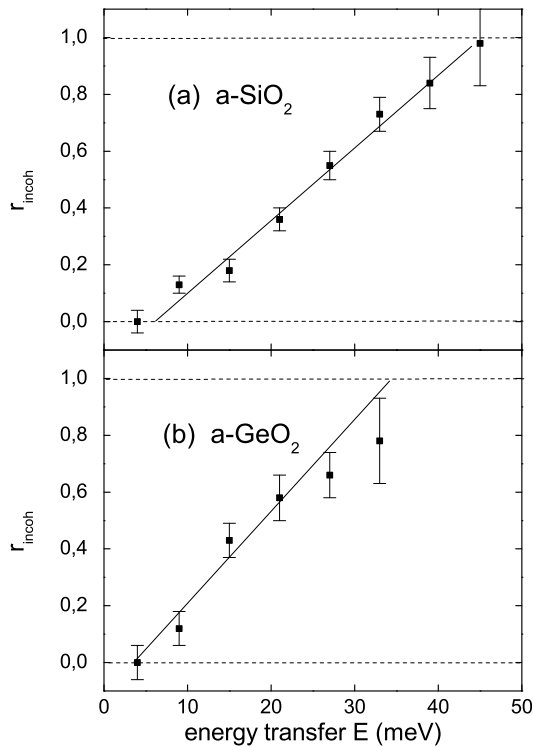


FIG. 7: The change of the incoherent fraction r_{incoh} of the oscillation function with increasing frequency for (a) vitreous silica (b) vitreous germania.

momentum transfer region of the three measurements. One can use it to replace the incoherent approximation $S_{boson}(Q) = 1$. Fig. 4 (a) shows that it gives a much better agreement with experiment than the incoherent approximation, at least in the frequency region of the boson peak.

As one goes up in frequency, the oscillations of the measured dynamic structure factor begin to get weaker, until one reaches again the incoherent approximation at about 40 meV (see Figs. 5(a) to (c)). One can follow this behaviour quantitatively by fitting the inelastic intensities in subsequent frequency windows in terms of the oscillation function

$$S_\omega(Q) = r_{incoh}(E) + [1 - r_{incoh}(E)] S_{boson}(Q) \quad (15)$$

where $S_{boson}(Q)$ is the five-lorentzian fit of Fig. 4 and $r_{incoh}(E)$ is the energy-dependent fraction of incoherent scattering, going from 0 to 1 as one goes from the boson peak up to higher frequencies (Fig. 7 (a)). Fig. 5 shows that one obtains a good fit of the measurements in this way. So within experimental accuracy, the peaks in the coherent inelastic dynamic structure factor of silica do not shift; they merely fade away to make room for a full validity of the incoherent approximation above 40 meV.

It is interesting to note that this crossover into a validity of the incoherent approximation occurs at the Debye frequency ω_D of vitreous silica. Debye's strongly oversimplified picture describes the whole vibrational density of states in terms of sound waves. The total density of sound waves (normalized to 1) is

$$g(\omega) = \frac{3\omega^2}{\omega_D^3}, \quad (16)$$

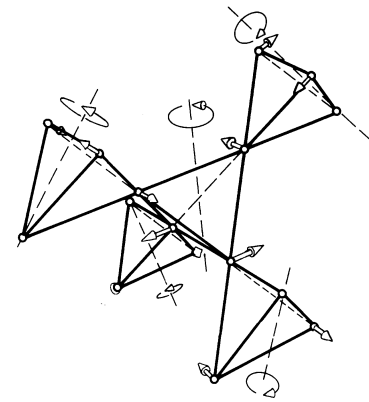


FIG. 8: Coupled libration of five corner-connected SiO_4 - or GeO_4 -tetrahedra⁶.

TABLE I: Debye frequencies of vitreous silica and germania⁴.

substance	\bar{M} a.u.	ρ kg/m ³	v_l m/s	v_t m/s	$\hbar\omega_D$ meV
$a - SiO_2$	20	2200	5800	3800	42
$a - GeO_2$	34.86	3600	3680	2410	26.8

with the Debye frequency ω_D given by

$$\omega_D^3 = \frac{18\pi^2\rho}{\bar{M}(1/v_l^3 + 2/v_t^3)}. \quad (17)$$

Here ρ is the density, v_l is the longitudinal sound velocity and v_t is the transverse sound velocity. Table I gives the values for vitreous silica and germania.

In germania, the oscillations of the inelastic dynamic structure factor fade even more quickly with increasing frequency than in silica (Fig. 7 (b)). Again, the validity of the incoherent approximation is reached at about the Debye frequency.

Having established the frequency dependence of the dynamic structure factor in both glasses, we proceed to the second step, the understanding of the oscillation function $S_{boson}(Q)$ at the boson peak in terms of a detailed picture of the atomic motion.

To find such an understanding, let us first recall what one knows about this frequency region, both from the quartz crystal^{16,17} and from the silica glass neutron^{6,8} and Hyperraman¹⁸ studies. One expects a mixture of long-wavelength sound waves and SiO_4 -tetrahedra libration. The oscillation function of the translational motion of long-wavelength sound waves¹⁹ is $S(Q)$. The oscillation function $S_{rot}(Q)$ of the coupled tetrahedra libration was calculated from the motional model of Fig. 8, using eq. (11) for $S_\omega(Q)$ in the one-phonon approximation.

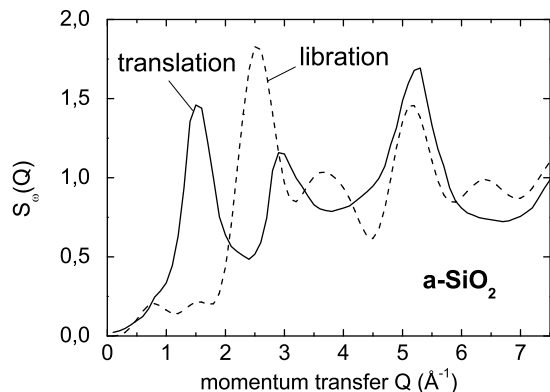


FIG. 9: Comparison of the translation oscillation function $S(Q)$ (continuous line) with the oscillation function $S_{rot}(Q)$ (dashed line) of the coupled libration of five corner-connected SiO_4 -tetrahedra⁶ of Fig. 8.

Fig. 9 compares the two oscillation functions $S(Q)$ and $S_{rot}(Q)$ for silica. They differ mainly at the first and second peak. Thus a strong first peak in $S_{boson}(Q)$ means a large sound wave fraction in the boson peak modes, a strong second peak a large tetrahedra libration fraction.

Fig. 6 (a) shows the best fit (continuous line) of the observed $S_{boson}(Q)$ of silica in terms of a sum of the two oscillation functions. The fit is by no means perfect, but supplies a fraction of 0.55 of tetrahedra libration signal and 0.45 of translation.

This is a surprising result. If one estimates the strength of the translational signal on the basis of the Debye sound-wave treatment, one would expect no more than a translational fraction of 0.2 at the boson peak^{6,8}. Similarly, the Hyperraman data¹⁸ require a dominating role of the tetrahedra libration for their understanding. But obviously, the librational motion of the corner-connected tetrahedra is accompanied by strong translational shifts.

A similar effect appears in germania. The fit in terms of a sum of the $S(Q)$ of germania and the tetrahedra libration (the line in Fig. 6 (b)) gives an even larger fraction of 0.75 for $S(Q)$. As we will see, the Debye expectation in germania is again a factor of two smaller. We will come back to this point in the discussion.

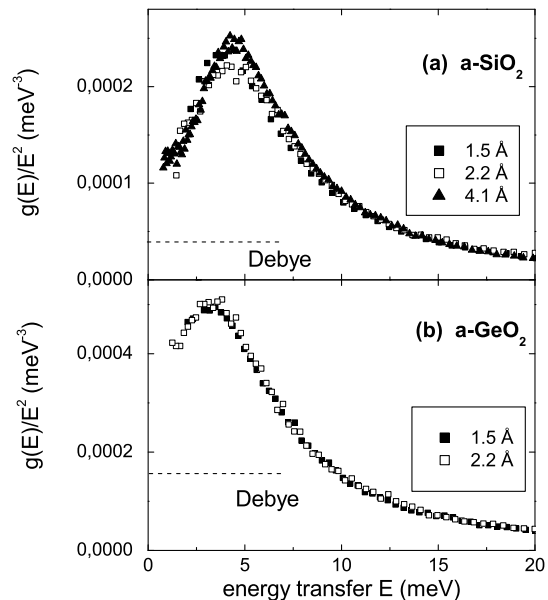


FIG. 10: Vibrational density of states (plotted as $g(E)/E^2$ to emphasize the boson peak at 4 meV), obtained using the extended approximation for (a) the three time-of-flight datasets of vitreous silica (dashed line: Debye expectation) (b) the two IN4 measurements of vitreous germania (dashed line: Debye expectation).

C. Vibrational density of states in the extended approximation

If one knows what kind of vibrational modes one deals with, one can calculate the vibrational density of states in the extended approximation, accounting for the cross sections and amplitudes of the atoms participating in the modes.

For vitreous silica, we take the signal at the boson peak to consist of 55 % of tetrahedra libration signal and 45 % of $S(Q)$, the result of the best fit of the data in Fig. 6 (a). Since the tetrahedra libration is essentially oxygen motion, we have to correct the number of resulting modes dividing by the enhancement factor for a pure oxygen motion

$$f_O = \frac{\sigma_O}{\bar{\sigma}} \frac{\bar{M}}{M_O} = 1.49, \quad (18)$$

where σ_O is the oxygen cross section and M_O is the oxygen mass. $\bar{\sigma}$ and \bar{M} are the average values of cross section and mass as defined in Section II.

The increasing incoherent fraction r_{incoh} of $S_{dyn}(Q)$ in eq. (15) is taken to be an average motion of all atoms, which requires no enhancement factor.

With these assumptions, one can determine a vibrational density of states from the data using the extended approximation, eq. (10). $S_{boson}(Q)$ is calculated from the sum of 45 % of $S(Q)$ and 55 % of the tetrahedra libration oscillation function $S_{rot}(Q)$ of the model in Fig. 8. $S_\omega(Q)$ is evaluated from eq. (15), taking r_{incoh} to follow the line in Fig. 7.

Fig. 10 (a) shows the vibrational density of states of vitreous silica obtained in this way for the three sets of data, plotted as $g(E)/E^2$ to emphasize the boson peak at 4 meV.

For vitreous germania, we take the signal at the boson peak to consist of 25 % of tetrahedra libration signal and 75 % of $S(Q)$. Again, we have to correct the number of resulting modes dividing by the enhancement factor for a pure oxygen motion

$$f_O = \frac{\sigma_O}{\bar{\sigma}} \frac{\bar{M}}{M_O} = 1.59. \quad (19)$$

The resulting vibrational density of states $g(E)/E^2$ is shown in Fig. 10 (b).

V. DISCUSSION

A. Potential and limitations of the method

Let us begin the general discussion with a disclaimer: The evaluation method for coherent inelastic neutron or x-ray scattering from glasses proposed in the present paper, which we denote by "extended approximation", is by no means new. Its beginnings can be traced back to the classical paper of Carpenter and Pelizzari¹⁹ (and

even beyond that). In a less formal way, it has been applied earlier, not only to vitreous silica^{6,8}, but also to amorphous germanium²⁰, deuterated polybutadiene²¹ and boron trioxide²². Our present work merely formalizes this extended approximation, introducing the concept of the oscillation function $S_\omega(Q)$ and giving a recipe for its experimental determination.

The oscillation function $S_\omega(Q)$ contains information on the eigenvector of the vibrational or relaxational modes seen at the frequency ω . The information is limited: Even if one knows $S_\omega(Q)$ with high accuracy over a large Q -range, one cannot determine the eigenvectors at that frequency. One can only check models of the motion against the measured $S_\omega(Q)$. In a practical sense, even such a check is restricted to the use of the one-phonon approximation of eq. (11), because it is difficult to calculate the interference oscillations of the coherent multiphonon scattering. Fortunately, the one-phonon approximation holds to rather large momentum transfer at the boson peak, the most interesting target for these studies.

At the boson peak, the analysis is simplified by the scientific question: one wants to know (i) whether the long-wavelength sound waves at the boson peak frequency still follow the Debye expectation (ii) whether there are additional modes, and if there are, what their eigenvector is. The first of these questions can be attacked, using the fact¹⁹ that the oscillation function $S_\omega(Q) \Rightarrow S(Q)$ for long-wavelength sound waves, no matter whether they are transverse or longitudinal. The second requires a model calculation for whatever mode is expected to be soft in the given system. In our cases silica and germania, one expects the coupled libration of corner-connected tetrahedra to be soft, because this is the soft mode of the phase transformation from α to β in crystalline quartz¹⁶.

Note that this rather streamlined procedure has weak points: (1) since the sound waves interact with the additional modes^{23,24}, one needs the $S_\omega(Q)$ of the resulting true eigenmodes, in which translation and soft mode eigenvector parts have a nonzero interference term. Therefore their $S_\omega(Q)$ might be different from a simple sum of the two oscillation functions. (2) At the boson peak, measurements of incoherent scatterers^{25,26} reveal sizeable nongaussianity effects. These will tend to distort the experimental $S_\omega(Q)$, determined on the basis of the Gaussian approximation.

In view of these points, it is not surprising that the agreement between the model calculation and the data in Fig. 6 (a) and (b) is not perfect. Nevertheless, the comparison with heat capacity data in the next subsection shows the reliability of the resulting vibrational density of states.

The extended approximation should be particularly useful for the evaluation of wide-angle inelastic x-ray scattering data. Such measurements have been reported^{27,28}, but have not been evaluated on a quantitative level. With the recipe given here, one could do a quantitative evaluation, provided one has good x-ray diffraction measurements. In that case, one even could

do only constant-Q scans (simpler to measure than the constant-E scans of the two references^{27,28}), relating their intensities by the diffraction measurement.

B. Comparison to heat capacity

We want to check the vibrational density of states obtained in the previous section from the extended approximation against earlier results in the literature. The first check is against heat capacity data from silica⁶ and germania²⁹ between 1 and 20 K. If one plots the heat capacity C_p as C_p/T^3 , one gets a close correspondence to the plot of $g(E)/E^2$, showing the boson peak of silica and germania at about 10 K.

In this comparison, the mode eigenvector assignment at the boson peak is checked, because the assumed fraction of tetrahedra libration provides the correction to the number of vibrational modes.

Fig. 11 (a) compares measured heat capacity data⁶ of vitreous silica to the result of the evaluation of the neutron data in the extended approximation, described in the preceding section. We chose the results from the measurement at 4.1 Å, because the heat capacity measurements⁶ stem from the same sample. As it turns out, the correction of the enhancement factor of eq. (18) is essential to get good agreement. So the comparison

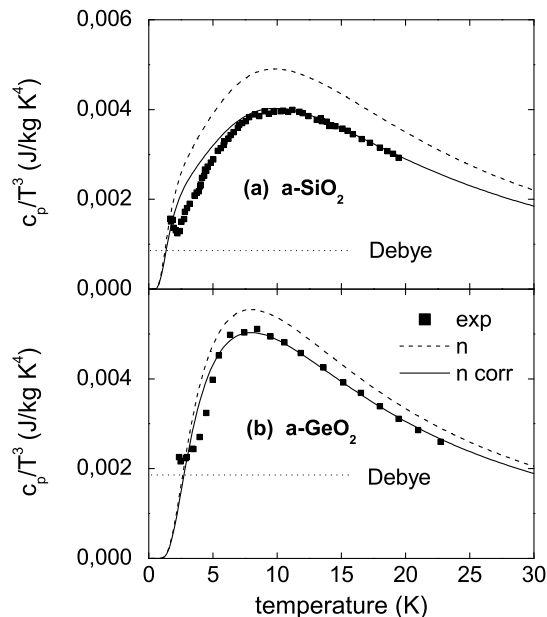


FIG. 11: Comparison of the heat capacity calculated from the neutron data with and without correction for the enhancement factor of the tetrahedra librational modes (the one without correction is close to the result from the incoherent approximation) to measured data (a) of vitreous silica⁶ (b) of vitreous germania²⁹.

corroborates the assignment of 55 % pure oxygen signal and 45 % translational signal at the boson peak in vitreous silica.

Similarly, Fig. 11 (b) shows good agreement between measured²⁹ and calculated heat capacity data in vitreous germania. Here, we compare to the 2.2 Å measurement, because it has the better resolution. Again, the correction improves the agreement. However, in this second case the correction is smaller, because according to the fit of the measured dynamic structure factor of Fig. 6 (b) we have only 25 % tetrahedra libration at the boson peak. Again, this conclusion is supported by the heat capacity data.

C. Comparison to simulation

There is a large number of molecular-dynamics simulations of vitreous silica in the literature^{30,31,32}, most of them done with effective classical force fields like the BKS potential³³. The BKS potential reproduces the measured $S(Q)$, but a recent comparison to an *ab initio* calculation³⁴ shows that it fails not only to reproduce the vibrational density of states, but also the mode eigenvectors.

Fig. 12 compares the vibrational density of states determined from the neutron measurement at 4.1 Å in the extended approximation with the *ab initio* calculation³⁴ and with an earlier neutron determination with very short wavelength at the spallation source at Argonne⁷. Note that the two neutron determinations are complementary: the spallation source measurement suffers from an overcorrection at low frequencies, but provides a true picture of the high-frequency density of states. In contrast, the cold neutron measurement is unable to measure above 100 meV, but provides good results at low frequency, as shown by the comparison to the low-temperature heat capacity data in the previous subsection.

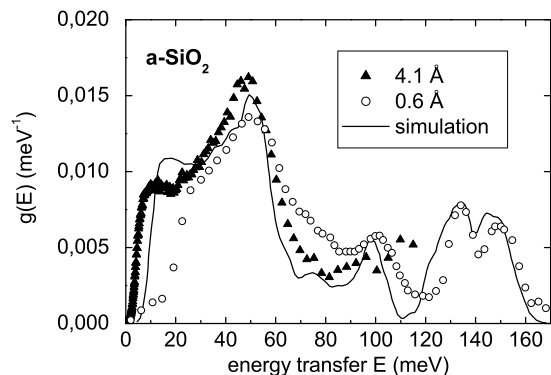


FIG. 12: Vibrational density of states of vitreous silica from an *ab initio* simulation³⁴, from earlier neutron work⁷ with 0.6 Å and from the present evaluation of the 4.1 Å data.

tion. Between 20 and 100 meV, the two sets of data agree reasonably well with each other.

Note that the *ab initio* simulation is unable to describe the boson peak region below 10 meV. Above that region, there is impressive agreement between simulation and neutron experiment. But below 10 meV, the simulated modes fail to come down to the low frequencies where both neutrons and heat capacity report them to exist. The reason might be either the small size of the simulation cell or its poor equilibration, natural disadvantages of an *ab initio* simulation.

It is interesting to compare our results to a simulation²⁴ of dynamic structure factors of a different system, soft spheres interacting with a repulsive $1/r^6$ potential, a model appropriate for metallic glasses. In this case, the oscillation function at the boson peak shows only the peaks of $S(Q)$. The additional modes seem to be a motion along a chain of nearest atomic neighbors, with an oscillation function which resembles $S(Q)$. This is obviously different in silica and germania, where the resonant boson peak modes seem to have a distinct tetrahedra rotation component.

D. Sound waves at and above the boson peak

The preceding two subsections demonstrated the ability of the extended approximation to determine a reliable vibrational density of states, in particular in the frequency region of the boson peak. This good agreement supports the interpretation of the boson peak modes as a mixture between long-wavelength sound waves and soft modes, in the cases of silica and germania librational modes of corner-connected tetrahedra.

But the sound-wave fraction determined from the dynamic structure factor is decidedly higher than the expectation on the basis of the sound-wave Debye model. Looking at the boson peak region between 2 and 6 meV in Fig. 10 (a) and (b) and the dashed line of the Debye expectation, one would expect no more than 20 % sound waves in silica and no more than 40 % in germania. The fit of $S_{boson}(Q)$ gives about twice as much in both substances. This finding goes beyond earlier cold-neutron work^{6,8}, which could not quantify the sound wave fraction at the boson peak.

The effect is apparently not limited to silica and germania. Earlier decompositions of $S(Q, \omega)$ at the boson peak window into a Q^2 - and a $Q^2S(Q)$ -part in deuterated polybutadiene²¹ and in vitreous B_2O_3 ²² also observed a larger $Q^2S(Q)$ -part than expected on the basis of the Debye model.

If the $Q^2S(Q)$ part is only due to sound waves, this implies a downward shift in frequency of the sound wave intensity above the boson peak. For the longitudinal sound waves, such a downward shift, together with a strong broadening, is in fact observed experimentally in x-ray Brillouin scattering³⁵. The broadening and the shift increase with the square of the phonon wavevector, i.e.

with the square of the nominal frequency of the phonon.

There is general agreement that the downward shift is not due to a dispersion of the sound velocity, but rather to sound wave scattering. One finds no evidence for any dispersion of either the longitudinal or the transverse sound velocity in tunneling diode³⁶ or ballistic phonon-pulse³⁷ experiments in vitreous silica and other glasses.

Also, there seems to be general agreement that the broadening of the sound waves observed in x-ray Brillouin scattering is not due to a true anharmonic damping of the sound waves, but rather to a deviation of the true eigenvectors from a purely sinusoidal displacement in space³¹.

On the other hand, there is a hot debate on the proper description of the x-ray Brillouin data, whether one should use a damped harmonic oscillator³⁵ (DHO) or whether one should take another form³⁸ which brings no intensity down to the frequency zero. But both forms shift the intensity down to lower frequencies, consistent with our observation of a heightened $Q^2S(Q)$ -component at the boson peak (heightened with respect to undamped Debye phonons).

The low-temperature plateau in the thermal conductivity⁴ and the phonon-pulse experiments³⁷ suggest that the transverse phonons have essentially the same fate as the one observed for the longitudinal phonons in x-ray Brillouin scattering^{35,38}.

To test these ideas, we submitted a Debye density of states with a Debye frequency corresponding to an energy

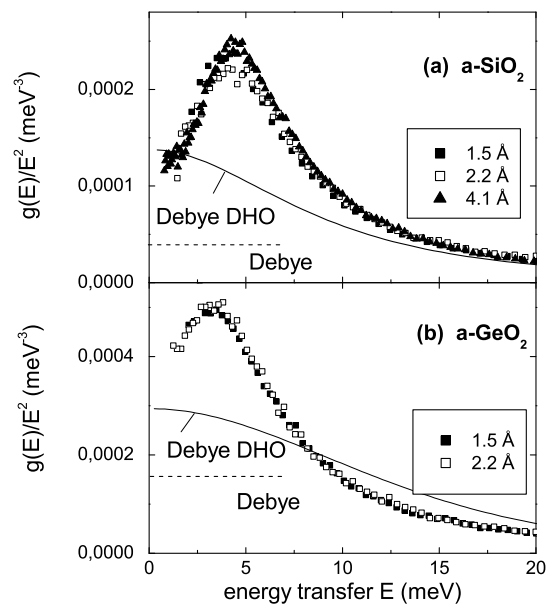


FIG. 13: Experimental density of states, plotted as $g(E)/E^2$ as in Fig. 10, compared to the simple Debye expectation (dashed line) and to Debye sound waves with DHO damping as explained in the text (continuous line) for (a) vitreous silica (b) vitreous germania.

transfer of 42 meV (the value for silica) to a DHO damping with the parameters of Benassi *et al*³⁵. The transverse phonons were assumed to have the same damping as the longitudinal ones at the same frequency, increasing proportional to the square of the phonon wavevector. The resulting effective Debye density of states is shown as the continuous line in Fig. 13 (a). To do the same calculation for germania, shown in Fig. 13 (b), we used recent neutron Brillouin measurements³⁹. According to them, the strong damping condition $\Gamma = v_l q$ (q phonon wavevector) is reached at the energy transfer 19.3 meV, a bit less than three quarters of the Debye frequency. From Benassi *et al*³⁵, the same condition is reached in vitreous silica already at 12 meV, at about only one quarter of the Debye frequency.

Fig. 13 shows that the scattering of the sound waves is strong enough to have a non-negligible effect on their spectral appearance in a scattering experiment. But it also shows that one cannot explain the boson peak in terms of the sound wave scattering alone. This does not depend on the choice of the DHO. If one takes the alternative proposed by the Montpellier group³⁸, one does indeed get a peak, because this alternative shifts the intensity to a finite frequency, not to the frequency zero. But the intensity of the peak remains too small. What one really needs is a mechanism which raises the total vibrational mean-square displacement by nearly a factor of two over the Debye expectation, a mechanism which brings vibrations from higher frequencies down to the boson peak. In vitreous silica and vitreous germania, one has the additional advantage that one can identify these additional vibrations by their dynamic structure factor.

VI. SUMMARY

We introduce a formal treatment of the coherent inelastic neutron or x-ray wide-angle scattering from glasses, which takes the interference oscillations explicitly into account. This "extended approximation" is an extension of the incoherent approximation. It allows to fit a newly defined "oscillation function" $S_\omega(Q)$ at each frequency ω , thus supplying information on the vibrational eigenvectors. The method should be particularly useful for the quantitative evaluation of wide-angle inelastic x-ray scattering measurements.

The application of the method to new room-temperature thermal neutron time-of-flight measurements of silica and germania not only provides a vibrational density of states in excellent agreement with heat capacity and simulation data, but also allows to quantify for the first time the ratio of tetrahedra rotation and tetrahedra translation at the boson peak. One finds about twice as much translation as in a simple Debye expectation. This excess is probably connected to the heavy damping of the sound waves at frequencies above the boson peak, observed by x-ray Brillouin scattering.

Acknowledgments

Thanks are due to Herbert Schober and Andreas Wischnewski for a critical reading of the manuscript.

* Electronic address: buchenau-juelich@t-online.de

¹ W. Marshall and S. W. Lovesey, *Theory of Thermal Neutron Scattering*, Oxford, Clarendon Press 1971

² N. V. Surovtsev, J. A. H. Wiedersich, V. N. Novikov, E. Rössler and A. P. Sokolov, *Phys. Rev. B* **58**, 14888 (1998)

³ J. Wiedersich, S. V. Adichtchev and E. Rössler, *Phys. Rev. Lett.* **84** 2718 (2000)

⁴ R. C. Zeller and R. O. Pohl, *Phys. Rev. B* **4**, 2029 (1971); M. P. Zaitlin and A. C. Anderson, *Phys. Rev. B* **12**, 4475 (1975); J. E. Graebner, B. Golding and L. C. Allen, *Phys. Rev. B* **34**, 5696 (1986); C. C. Yu and J. J. Freeman, *Phys. Rev. B* **36**, 7620 (1987)

⁵ F. Sette, M. Krisch, C. Masciovecchio, G. Ruocco and G. Monaco, *Science* **280**, 1550 (1998)

⁶ U. Buchenau, M. Prager, N. Nücker, A. J. Dianoux, N. Ahmad and W. A. Phillips, *Phys. Rev. B* **34**, 5665 (1986)

⁷ J. M. Carpenter and D. L. Price, *Phys. Rev. Lett.* **54**, 441 (1985)

⁸ A. Wischnewski, U. Buchenau, A. J. Dianoux, W. A. Kamitakahara and J. L. Zarestky, *Phys. Rev. B* **57**, 2663 (1998)

⁹ M. Nakamura, M. Arai, T. Otomo, Y. Inamura and S. M. Bennington, *J. Non-Crystalline Solids* **293-295**, 377 (2001)

¹⁰ M. Nakamura, M. Arai, Y. Inamura, T. Otomo and S. M. Bennington, *Phys. Rev. B* **67**, 064204 (2003)

¹¹ M. Russina, F. Mezei, R. Lechner, S. Longeville and B. Urban, *Phys. Rev. Lett.* **84**, 3630 (2000)

¹² W. Schmidt, M. Ohl and U. Buchenau, *Phys. Rev. Lett.* **85**, 5669 (2000)

¹³ P. A. V. Johnson, A. C. Wright and R. N. Sinclair, *J. Non-Cryst. Solids* **58**, 109 (1983)

¹⁴ C. E. Stone, A. C. Hannon, T. Ishikawa, N. Kitamura, Y. Shirakawa, R. N. Sinclair, N. Umesaki and A. C. Wright, *J. Non-Cryst. Solids* **293-295**, 769 (2001)

¹⁵ K. Suzuya, D. L. Price, M.-L. Saboungi and H. Ohno, *Nucl. Instr. and Meth. B* **133**, 57 (1997)

¹⁶ H. Grimm and B. Dorner, *J. Phys. Chem. Solids* **36**, 407 (1975)

¹⁷ H. Schober, D. Strauch, K. Nützel and B. Dorner, *J. Phys.: Condens. Matter* **5**, 6155 (1993)

¹⁸ B. Hehlen, E. Courtens, R. Vacher, A. Yamanaka, M. Kataoka and K. Inoue, *Phys. Rev. Lett.* **84**, 5355 (2000)

¹⁹ J. M. Carpenter and C. A. Pelizzari, *Phys. Rev. B* **12**, 2391 (1975)

²⁰ U. Buchenau, M. Prager, W. A. Kamitakahara, H. R. Shanks and N. Nücker, *Europhys. Lett.* **6**, 695 (1988)

²¹ U. Buchenau, A. Wischnewski, D. Richter and B. Frick,

- Phys. Rev. Lett. **77**, 4035 (1996), Fig. 4 (a)
- ²² D. Engberg, A. Wischniewski, U. Buchenau, L. Börjesson, A. J. Dianoux, A. P. Sokolov and L. M. Torell, Phys. Rev. B **58**, 9087 (1998)
- ²³ H. R. Schober and C. Oligschleger, Phys. Rev. B **53**, 11469 (1996)
- ²⁴ H. R. Schober, J. Phys.: Condens. Matter **16**, S2659 (2004)
- ²⁵ T. Kanaya, Prog. Theor. Phys. Suppl. **126**, 133 (1997)
- ²⁶ U. Buchenau, C. Pecharroman, R. Zorn and B. Frick, Phys. Rev. Lett. **77**, 659 (1995)
- ²⁷ C. Masciovecchio, A. Mermet, G. Ruocco and F. Sette, Phys. Rev. Lett. **85**, 1266 (2000)
- ²⁸ O. Pilla, A. Cunsolo, A. Fontana, C. Masciovecchio, G. Monaco, M. Montagna, G. Ruocco, T. Scopigno and F. Sette, Phys. Rev. Lett. **85**, 2136 (2000)
- ²⁹ A. A. Antoniou and J. A. Morrison, J. Appl. Phys. **36**, 1873 (1965)
- ³⁰ S. N. Taraskin and S. R. Elliott, Phys. Rev. B **55**, 117 (1997); **56**, 8605 (1997)
- ³¹ R. Dell'Anna, G. Ruocco, M. Sampoli and G. Viliani, Phys. Rev. Lett. **80**, 1236 (1998)
- ³² J. Horbach, W. Kob and K. Binder, Eur. Phys. J. B **19**, 531 (2001)
- ³³ B. W. H. van Beest, G. J. Kramer and R. A. van Santen, Phys. Rev. Lett. **64**, 1955 (1990)
- ³⁴ M. Benoit and W. Kob, Europhys. Lett. **60**, 269 (2002)
- ³⁵ P. Benassi, M. Krisch, C. Masciovecchio, V. Mazzacurati, G. Monaco, G. Ruocco, F. Sette and R. Verbeni, Phys. Rev. Lett. **77**, 3835 (1996)
- ³⁶ M. Rothenfusser, W. Dietsche and H. Kinder, Phys. Rev. B **27**, R5196 (1983)
- ³⁷ T. C. Zhu, H. J. Maris and J. Tauc, Phys. Rev. B **44**, 4281 (1991); C. J. Morath, G. Tas, T. C. Zhu and H. J. Maris, Physica B **219-220**, 296 (1996)
- ³⁸ E. Rat, M. Foret, E. Courtens, R. Vacher and M. Arai, Phys. Rev. Lett. **83**, 1355 (1999)
- ³⁹ L. E. Bove *et al*, unpublished